Optics and Lasers in Engineering 172 (2024) 107830

Contents lists available at ScienceDirect

Optics and Lasers in Engineering

journal homepage: www.elsevier.com/locate/optlaseng

Connecting the microscopic depolarizing origin of samples with macroscopic measures of the Indices of Polarimetric Purity

Mónica Canabal-Carbia [a,*], Irene Estévez [a], Esther Nabadda [b], Enrique Garcia-Caurel [c], J.J. Gil [d], Razvigor Ossikovski [c], Andrés Márquez [e,f], Ignacio Moreno [b,g], Juan Campos [a], Angel Lizana [a]

[a] Grup d'Òptica, Departamento de Física, Universitat Autònoma de Barcelona, Bellaterra 08193, Spain
[b] Instituto de Bioingeniería, Universidad Miguel Hernandez de Elche, Elche 03202, Spain
[c] LPICM, CNRS, Ecole Polytechnique, Institut Politechnique de Paris, Palaiseau 91120, France
[d] Departmento de Física Aplicada, Universidad de Zaragoza, Pedro Cerbuna 12, Zaragoza 50009, Spain
[e] Departamento de Física, Ing. de Sistemas y T. Señal, Universidad de Alicante, Alicante 03080, Spain
[f] I.U. Física Aplicada a las Ciencias y las Tecnologías, Universidad de Alicante, Alicante 03080, Spain
[g] Departamento de Ciencias de Materiales, Óptica y Tecnología Electrónica, Universidad Miguel Hernandez, Elche 03202, Spain

ARTICLE INFO

Keywords:
Mueller matrices
Indices of Polarimetric Purity
Depolarizers
Biophotonics
Polarization

ABSTRACT

In this work we show how a specific set of three depolarizing observables, the Indices of Polarimetric Purity (IPP), P_1, P_2 and P_3, are ideal metrics to study the depolarization characteristic of media. We simulate different depolarizing scenarios, based on different depolarizing origins, and we study the corresponding IPP values. The simulations are based on the incoherent addition of multiple elemental polarizing elements, as ideal polarizers and/or retarders with different specific characteristics (orientation, retardance, transmittance, etc.). Further depolarizing scenarios are also studied by including the effect of ideal depolarizers. We show for the first time how by analyzing depolarizing systems through IPP we unravel two different depolarizing origins: isotropic and anisotropic depolarization, with meaningful physical interpretation. The former, isotropic depolarization is related to pure scattering processes, and mainly connected with P_3 observable. The later, anisotropic depolarization is originated by microscopic constituent elements showing polarimetric anisotropy (dichroic and/or birefringent elements with different characteristics) and anisotropic scattering produced by these elements, and mainly described by P_1 and P_2 observables. Both effects can be simultaneously observed in real samples and give us information of the processes that give rise to depolarization in light-matter interactions. The simulated results are experimentally validated by analyzing the depolarizing behavior, in terms of IPP, of diverse real samples with easy physical interpretation, and direct connection with simulations. The present study could be of interest in multiple scenarios, to further understand the depolarizing response of samples, and it can be of special interest for the study of biological tissues and pathologies, as they present important depolarizing behavior.

1. Introduction

Polarimetry encompasses a collection of optical techniques devoted to analyzing one main characteristic of transversal waves, the polarization, or the polarimetric property of samples, through light-matter interactions. Nowadays, polarimetry is useful in a wide range of applications, as in astronomy [1], remote sensing [2], material characterization and quality control [3,4], food analysis [5], botanical applications [6], biomedicine [7], among other.

In the case of biological samples, polarized light may be modified in different ways when interacting with different organic structures, this being of interest in terms of contrast enhancement between different structures in the samples. These differences in the exiting polarization after interacting with different tissues are related to the specific polarimetric characteristics of tissues, as the birefringence, dichroism, or depolarization. Typically, birefringence and dichroism are two polarimetric responses well-studied in biological samples, as it is common to find that constituent elements of tissues present some significant behavior in terms of birefringence or dichroism. For instance, in Ref. [8] the birefringent properties of a sample help to differentiate between healthy and cancerous tissue, in Ref. [9] elastic and collagen fibers in a rabbit aortic wall are characterized by its retardance, and in Ref. [10]

* Corresponding author.
E-mail address: monica.canabal@uab.cat (M. Canabal-Carbia).

https://doi.org/10.1016/j.optlaseng.2023.107830
Received 29 May 2023; Received in revised form 5 September 2023; Accepted 6 September 2023
Available online 20 September 2023

diattenuation allows to distinguish between brain regions with different tissue properties.

Depolarization is a measure of the sample capability to depolarize an incident fully polarized light beam. Traditionally, in terms of image contrast, depolarization was seen as a non-desired magnitude, which was tried to be minimized to exploit the other polarimetric properties. However, in the last decades, it has been revealed that depolarization channel itself provides large intrinsic information of samples (as for instance, organization, size, density of structures, etc.), as well as it is very relevant in terms of structures visualization enhancement. In this sense, depolarizing channels have been reported as useful to detect cancer stages in different human and animal tissues as *ex-vivo* human colon and skin [11,12] colon cancer, skin carcinoma, pathology detection in vegetal tissue [13] and, tissue recognition [14].

An ideal framework to study depolarizing properties of samples is the Mueller–Stokes (M-S) formalism. In this sense, the Mueller matrix of a sample, can be experimentally determined from intensity measurements. Different observables that can be deduced from the coefficients of the Mueller matrix allow to study the depolarizing properties of samples [15–17]. Among these different approaches, in this work we use the Indices of Polarimetric Purity (IPP) [18–20] as reference metrics to study the depolarization. The IPP comprises a set of three observables, the P_1, P_2 and P_3, channels, that can be derived from the eigenvalues of the covariance matrix [20] (a transformation of the Mueller matrix), and they are connected to the polarimetric randomness structure of the sample that they represent [21–23]. The IPP are an ideal framework to study the depolarizing properties of biological samples, as they have already proved their interest for the image enhancement and discrimination of biological structures [6,13,24,25] as well as to construct recognition models for the guided detection of biological structures [14].

In this work we take advantage of the IPP as a metrics to study the depolarization origin. For this purpose, we construct different depolarizers through the incoherent summation of different basic elements (pure diattenuators, pure retarders and perfect depolarizers), with different properties and orientations. The resulting simulated scenarios, studied in terms of IPP, allow us to understand the inherent constituents within samples with regards to their macroscopic depolarizing response. In this sense, the proposed simulations allow us to differentiate between different kind of depolarizers, arising two main depolarizing mechanisms: (1) depolarizers whose depolarizing response does not depend on the input state of polarization; and (2) depolarizers whose depolarizing response depends on the input polarization. Importantly, we demonstrate how those depolarizing vias can be quantified by using the IPP framework. In addition, the proposed simulated environments are experimentally validated with simple samples with well-defined polarization properties that reproduce phantom experiments.

The presented study allows us to connect inherent physical properties of samples with measurable depolarization data and it provides new analytical tools for a better understanding of depolarizing mechanisms in biological samples, and therefore, to their inherent structures.

2. Indices of Polarimetric Purity (IPP) as a framework to study depolarizing behavior of samples

In this section we provide the fundamentals necessary to construct the models given in further Section 3, which will help us to study different depolarizing scenarios.

In particular, we focus on the IPP to provide fundamental information about the origin of depolarization. The choice of the IPP is not arbitrary since they provide further information than other well-known depolarizing observables (as the Degree of Polarization or the Depolarizing index [27]) as well as because their interest for the enhanced visualization of tissues has already been demonstrated [13]. To study the IPP parameters we construct our simulations and experiments based on the M-S formalism [28,29]. In this formalism, the state of polarization of the light is described by the Stokes vector (***S***), whereas the polarimetric properties of samples are described by Mueller matrices (***M***) [17, 28–32].

In the following, we briefly review the calculation of the IPP. These three magnitudes arise naturally when applying the spectral theorem [33] on polarimetric systems. The IPP constitute a set of three real magnitudes, named P_1, P_2 and P_3, defined as combinations of the covariance matrix H (associated with M) eigenvalues (λ_i) [17,20,33]:

$$\begin{aligned} P_1 &\equiv \frac{\lambda_0 - \lambda_1}{TrH}, \\ P_2 &\equiv \frac{\lambda_0 + \lambda_1 - 2\lambda_2}{TrH}, \\ P_3 &\equiv \frac{\lambda_0 + \lambda_1 + \lambda_2 - 3\lambda_3}{TrH}, \end{aligned} \tag{1}$$

where, the values are restricted between 0 and 1, and follow the relation:

$$0 \le P_1 \le P_2 \le P_3 \le 1, (\mathrm{i} = 1, 2, 3) \tag{2}$$

Pure or non-depolarizing systems are characterized by P_1=P_2=P_3=*1*, while for totally or ideal depolarizers P_1=P_2=P_3=*0*.

Importantly, the characteristic decomposition of the Mueller matrix can be expressed in terms of the IPP as [19,20]:

$$\begin{aligned} M = {} & P_1(m_{00}\widehat{M}_{J0}) + (P_2 - P_1)(m_{00}\widehat{M}_1) + (P_3 - P_2)(m_{00}\widehat{M}_2) \\ & + (1 - P_3)(m_{00}\widehat{M}_3) \end{aligned} \tag{3}$$

where, P_1 is the weight of the nondepolarizing component $\widehat{M}_{J0}$, P_2-P_1 is the portion of the medium that behaves as a 2D depolarizer (represented by $\widehat{M}_1$), P_3-P_2 summarizes the part of the medium that behaves as a 3D depolarizer (represented by $\widehat{M}_2$), *1*-P_3 is the portion of the medium behaving as a perfect depolarizer where $\widehat{M}_3$=*diag(1,0,0,0)* and the circumflex in M denotes the normalized matrix in each case [17,19,30].

Note how Eq. (3) becomes very interesting because it allows us connecting the weights of the different terms of the characteristic decomposition, which are physically interpretable, with combinations of IPP, which can be experimentally obtained.

3. Depolarizing systems with P_3=*1*

Depolarizing behavior of samples can be understood as their ability to introduce polarimetric randomness to an input polarized light beam. When an expanded beam illuminates a sample, light-matter interactions are produced which result in heterogeneous modifications of the polarization spatial distribution of light. Those polarization spatial distributions are incoherently added at the detectors of polarimeters, leading to depolarization measurements. The physical origin behind the depolarizing response of a sample is multiple, but it is always connected to the inherent constituents of the sample, and how they modify polarization through light-matter interactions. In this work, we provide different cases of study which lead to depolarization, and they are very easy to interpret. The cases will be studied in terms of their Indices of Polarimetric Purity (IPP) values, because, as we will show, the IPP allow us to catalog different kinds of depolarizers as a function of the inherent processes that give rise to the depolarization.

To do so, we will model different depolarizer scenarios in which depolarization takes place, consisting of basic physical elements, this leading to a very simple interpretation of the depolarizing processes behind them. In particular, in this section we present two different simulations of depolarizers that are based on the simplest polarimetric elements: linear retarders and linear diattenuators. As it will be shown, these two scenarios lead to the particular value of P_3=*1*, whereas P_1 and P_2 are different from case to case. In Section 1.3 of the supplementary document, we also include the simulation where the Mueller matrix is constructed by the combination of linear diattenuators and retarders. The behavior of these M is similar to the ones presented in the main text,

and P_3=*1* for all the cases.

The models presented in the following are implemented in a way that is in adequacy with the premises of the parallel decomposition [17]. The latter decomposition states that, any depolarizing M can be described as an incoherent sum of Mueller matrices M_i [18,19,21,33,34]

$$M = m_{00}\widehat{M} = m_{00}\sum_{i}^{n}\alpha_i\widehat{M}_i; \alpha_i \geq 0; \sum_{i=1}^{n}\alpha_i = 1 \tag{4}$$

In this section, we conduct the simulations based on the incoherent addition of n Mueller matrices of pure polarimetric elements (linear diattenuators and linear retarders; with different values and orientations). These simulations pretend to mimic the macroscopic response of complex systems including dichroism, birefringence, or both.

3.1. Depolarizers originated by the incoherent addition of linear diattenuators

The first case of study consists of the simulation of depolarizers constituted by the incoherent addition of linear diattenuators. The Mueller matrix of a *x-y* aligned linear diattenuator M_{LD} can be written as [28]:

$$M_{LD}(p_x, p_y) = \frac{1}{2}\begin{pmatrix} p_x^2+p_y^2 & p_x^2-p_y^2 & 0 & 0 \\ p_x^2-p_y^2 & p_x^2+p_y^2 & 0 & 0 \\ 0 & 0 & 2p_xp_y & 0 \\ 0 & 0 & 0 & 2p_xp_y \end{pmatrix}; 0 \leq p_{x,y} \leq 1, \tag{5}$$

here p_x and p_y are the amplitude attenuation coefficients for the x and y components, respectively. To make the simulation more realistic, we will consider diattenuators oriented at different angles. To do so, we have to take into account the Mueller matrix of a rotator [28], where θ is the angle of the rotator. Therefore, the Mueller matrix of each linear diattenuator rotated to an angle θ can be obtained as [28]:

$$M(p_x, p_y, \theta) = M_{rot}(-\theta)M_{LD}M_{rot}(\theta). \tag{6}$$

Under this scenario, by applying the summation in Eq. (4) to Mueller matrices with the structure given in Eq. (6), we achieve a model with different control parameters: the number n of Mueller matrices in the summation, the amplitude coefficients (p_x and p_y) and the orientation angle (θ) for each Mueller matrix.

Therefore, we need a criterion to choose the way to assign different values to the parameters in each diattenuator within the summation. These values could be set arbitrarily, for instance, by generating random numbers, but to simulate a situation closer to real samples, such as the distribution of collagen fibers in a tendon or cellulose in the vascular tube of a leaf, we restrict the domain of variation. We consider a group of dichroic optical elements, with a privileged direction, with deviations from this direction. To do that, the values for the control parameters in each of the n matrices in the summation are assigned by $\overline{X} + \delta$, where $\overline{X}$ is the mean value parameter and δ is a random variable that follows a Gaussian distribution with a null mean and a given variance (σ). The mean values for the amplitude coefficients p_x, p_y are bounded within the range (0, 1) and the mean orientation of the diattenuators within the range (0,180º).

Afterwards, for the sake of interpretation (to limit the space of simulations), we chose to fix in all the simulations the value of the amplitude coefficient in the x direction p_x to a constant value. Regarding the number of elements in the incoherent addition, we set $n = 1500$, this number being a trade-off between a large number of elements (to mimic real processes of light-matter interaction) and a reasonable computation time.

Once we have set the values for p_x and n, our remaining control parameters are p_y and θ. For each value of p_x, we conduct a collection of simulations by taking a given value of p_x and changing the values of p_y from 0 to 1 with steps of *0.003* and with a null variance (σ_{py}=0), and values of $\overline{\theta}$ with a given mean value (we choose θ=60º and a variance (σ_θ) taking values from 0º to 180º with steps of 0.6º. This lead to a 300 x 300 = 90,000 simulations, each one leading to a Mueller matrix of a composed depolarizer. In order to study the depolarizing properties of the resulting 90,000 depolarizers, the IPP (i.e., P_1, P_2 and P_3 channels) values are calculated according to formulation given in Section 2.

The results obtained for P_1, P_2 and P_3 are presented in Fig. 1. The x axis provides the p_y parameter, whereas the y axis shows the values for the variance of $\overline{\theta}$, the σ_θ parameter. Therefore, the resulting images include the IPP values for the 90,000 simulations, each pixel of the image corresponding to a particular ($p_{y,i}$, σ_θ combination). The values for the IPP are coded in a color scale ranging from the minimum value (0 value, in blue) to the maximum value (1 value, in yellow), as provided by the colorbar. In addition, different rows in Fig. 1 provide the IPP simulations for two different values of p_x (0.8 and 0.2). We have also computed the simulations for different values of p_x, these results are presented in Section 1 of the supplementary material.

In Fig. 1(a)–(f) we observe the behavior of different depolarizers based on incoherent addition of linear diattenuators with different characteristics of (p_x, p_y, and σ_θ). Regarding the orientation angle mean value for the constituent diattenuators, σ_θ, this parameter is set as 60º for all simulations in Fig. 1. The choice of such angle was arbitrary as we have observed that simulations are independent of this parameter. In fact, the orientation angle does not affect the polarimetric characteristics of the resulting depolarizers since it can be understood as a rotation of the system, and thus, the enpolarizing and depolarizing properties of the simulated samples should be conserved.

Regarding data in Fig. 1(a)–(f), the first result we observe is that, independently of the model parameters (p_x, p_y, and σ_θ), the P_3 parameter always equals 1. Therefore, we cannot modify the P_3 value with this combination of diattenuators and the consequent depolarizers are always restricted to the top of the tetrahedron of the Purity Space [35]. As a consequence of this, we cannot achieve an ideal depolarizer (*diag(1,0, 0,0)*) by simply varying the parameter values in the diattenuation model. Indeed, the P_3 =1 plane does not contain the ideal depolarizer, and thus all the points on such a plane necessarily exhibit depolarizations strictly lower than the maximum one that is, depolarization cannot be continuously increased to the ideal depolarizer value.

Secondly, we note that the values of P_1 and P_2 channels are modified with different values of p_x, p_y, and σ_θ, and thus, the depolarizing response of resulting depolarizers strongly depend on these parameters. As P_3 is always equal to 1, this implies that different depolarizers (different pixels in images in Fig. 1(a)–(f)) correspond to different spatial positions at the plane P_3=1 in the Purity Space [35]. Therefore, the channels P_1 and P_2 are suitable tools to differentiate between different depolarizers originated by dichroic structures. Importantly, note the close similarity in the responses of P_1 and P_2 images. In fact, they present identical behavior for a fixed value of p_x (different rows), but P_2 presents a vertical shift upwards as p_x increases (from bottom to upper row). This situation can be explained by taking into account the inequality shown in Eq. (2), which forces P_2 to have larger (or equal) values than P_1. In turn, we also observe that larger σ_θ values (vertical axis) lead to smaller values for P_1 and P_2. In fact, for σ_θ =0 we obtain P_1=P_2=P_3=*1* (yellow color) in all the cases, and P_1 and P_2 tend to decrease their values as σ_θ increase. This situation implies that the larger the loss of organization for the constituent units (diattenuators) (i.e., σ_θ increase), the larger the depolarizing capability of the system (i.e., P_1 and P_2 decrease). Note that this behavior is observed until a certain limit value for σ_θ, that depends on the p_x value (different rows) but in general it occurs around $\sigma_\theta = 40º$ both for P_1 and P_2 metrics. This implies that even increasing the disorder of polarizing units constituting samples, there is a certain limit from which depolarizing response of samples is not modified anymore. The existence of this limit can also be discussed in an intuitive and visual way in terms of the Purity Space, as presented in the Supplementary material

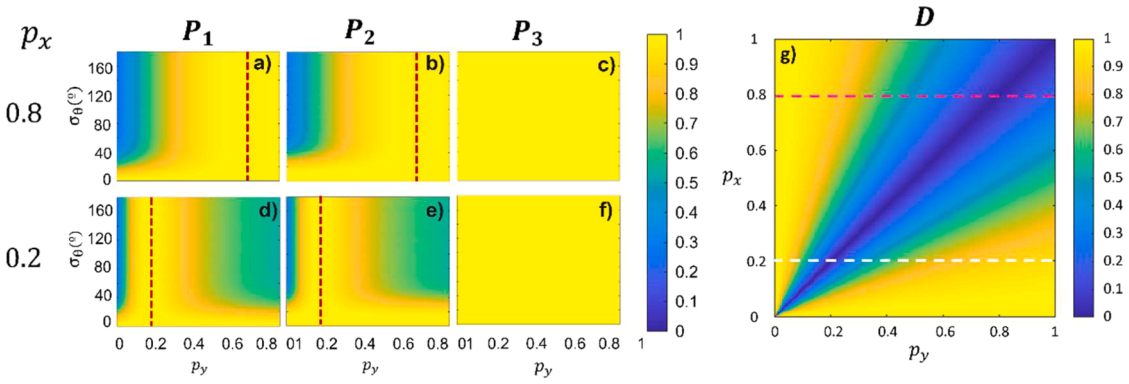

Fig. 1. (a)–(f) IPP values for simulated samples composed by incoherent additions of linear diattenuators. The x axis represents the mean values of p_y and, the y axis the values for σ_θ . The value of p_x is set as a constant for each image, with values of 0.8 and 0.2, respectively for the two different rows. The value of the mean orientation angle $_\theta$ is set as 60° for all cases. (g) D value for the incoherent addition of linear diattenuators with $\sigma_\theta = 0$, the x and y axis represent the p_x and p_y parameters, defined in the range 0 to 1.

(Section 5).

This set of simulations can also be studied in terms of the diattenuation D observable, representing the dependence of the sample transmittance with the state of polarization of the incident light. The diattenuation D can be calculated as the absolute value of the diattenuation vector, which can be written in terms of the first row Mueller matrix elements in the following way [28]:

$$D = \frac{1}{m_{00}}(m_{01}, m_{02}, m_{03})^T. \tag{7}$$

If we substitute in Eq. (7) the elements of the Mueller matrix correspondent to a general diattenuator (Eq. (5)), the absolute value of the diattenuation vector, D, can be expressed as [17]:

$$D = \frac{\left|p_x^2 - p_y^2\right|}{p_x^2 + p_y^2}. \tag{8}$$

Note that the diattenuation parameter D is a significant feature of diattenuators, taking values of $D = 1$ for an ideal diattenuator, and values of $D = 0$ for a medium with no diattenuation.

Taking the definition of D in mind, and back again to Fig. 1(a)–(f), we find a non-depolarizing zone (yellow color) when p_x=p_y (indicated with a red dotted line in each image). According to Fig. 1(g) this situation corresponds to values of $D = 0$ (see positive diagonal in blue), and therefore, non polarimetric elements (thus without the capability of enpolarize and depolarize). This condition leads to simulations based on the incoherent addition of media represented by the identity matrix, and as a consequence, without the potential of implementing depolarizers (see red dotted line in Fig. 1(a)–(f)). However, for $p_x \neq p_y$, the units of the incoherent addition present certain diattenuation (i.e., $D \neq 0$) (see Fig. 1 (g)), which leads to systems with certain depolarizing response. This depolarization response directly depends on the organization disorder (σ_θ) (see vertical axis in Fig. 1(a)–(g)).

The dependence of the IPP with the p_x and p_y values is easily understood by studying Fig. 1(g). The pink and the white dashed lines in the figure, indicate the D value for p_x=*0.8* and p_x=*0.2*, respectively, with p_y taking values from 0 to 1. Following the dashed white line in Fig. 1(p), the value of D is maximum for p_y=*0* and start to decrease as p_y increases, reaching the minimum for p_y=*0.2* (i.e., p_x=p_y). As p_y increases, the value of D increases as well, reaching the $D = 1$ value. This behavior explains the depolarization results obtained from Fig. 1(d) and (e), where P_1=P_2=*1* (non depolarizing scenarios) correspond to values of D equal or very close to zero (i.e., corresponding to the blue diagonal in Fig. 1 (g)), whereas for the situations where D reaches its maximum of high values, the depolarization capability of the samples increase, achieving values of P_2 and P_1 different from 1. The pink line indicates the case for p_x= 0.8. If we study the D behavior through this line, we can see that D is equal to 1 (or near) when the values of p_y are in the range (0,0.3). This corresponds with the left zone of the images where p_y is in the mentioned range and, we can see that in this case, for σ_θ values higher than the limit, the system depolarizes anisotropically. However, as p_y increases (D decreases) the depolarizing capability of the system is lost because the system becomes less dichroic.

Results shown in Fig. 1(g) corresponds with the case of σ_θ =0. We have also tested other values for the standard deviation of the mean orientation of the diattenuators and results and discussion are provided in the supplementary Material. The main conclusions are that the general structure shown in Fig. 1(g) is maintained, but the diattenuation values decrease with σ_θ, reaching a limit scenario, where diattenuation is equal to 0 for $\sigma_\theta \geq 40°$. This result has sense because as larger the deviation of θ, as larger the depolarizing capability of the depolarizer consisting of dichroic unitary elements.

Summarizing, in this subsection we have mimicked multiple depolarizers consisting of dichroic microscopic elements. As expected, incoherent addition of isotropic (in terms of dichroism) units (i.e., p_x=p_y scenario), lead to non-depolarizing samples (i.e., P_1=P_2=P_3=*1*). In turn, in the case of anisotropic elements ($p_x \neq p_y$), the resulting systems become depolarizers, and their depolarization capability increases for larger diattenuation D values (which depends on the p_x and p_y relation) of the constituent diattenuators, as well as with the units orientation disorder σ_θ. Importantly, the value of P_3 is independent of all the model parameters, and it maintains a constant value of P_3=*1* for all the simulations, and therefore, all depolarizers consisting of collections of linear diattenuators are placed into a specific plane of the Purity Space [35].

3.2. *Depolarizers originated by the incoherent addition of linear retarders*

The second study considers depolarizers consisting of microscopic unit elements presenting linear retardance. We proceed in analogy to the previous study corresponding to diattenuation, building in this case models consisting in the incoherent sum of sets of retarders as a function of their retardation and orientation. In Ref. [36] it is shown how the incoherent addition of linear retarders can also be performed analytically. We show the Mueller matrix for a linear retarder oriented at 0° [28]:

$$M_{LR} = \begin{pmatrix} 1 & 0 & 0 & 0 \\ 0 & 1 & 0 & 0 \\ 0 & 0 & \cos\phi & \sin\phi \\ 0 & 0 & -\sin\phi & \cos\phi \end{pmatrix}; 0 \leq \phi \leq \pi, \tag{9}$$

where, ϕ is the phase shift introduced to the orthogonal components of the incident light field. As in the previous case, to make simulations more realistic, we consider an ensemble of retarders oriented at different

angles, according to the relation $M = M_{rot}(-\theta)M_{LR}M_{rot}(\theta)$. For the incoherent sum of Mueller matrices of retarders, we consider a mean orientation ($\overline{\theta}$) for the retarders with a standard deviation (σ_θ) following a probabilistic Gaussian distribution. In addition, we vary the retardance value ϕ from 0º to 360º and with a null variance. As in the previous case, the obtained simulations (which are functions of ϕ and σ_θ) are interpreted in terms of the P_1, P_2, P_3 metrics.

In Fig. 2 we present the three IPP metrics corresponding to the simulations with linear retarders. The *x* axis represents the mean values of retardance ϕ, taking values from 0º to 360º, whereas the *y* axis represents the variance range from the mean orientation value, σ_θ, which can take values from 0º to 180º. For each of the possible values of ϕ we build the *M* corresponding to the incoherent sum of $n = 1500$ Mueller matrices where each of them has a value of orientation with a variance given by a Gaussian distribution. This process is repeated for the possible values of ϕ and σ_θ, both can take 300 different values within their respective ranges, this leads to 300×300 (90,000) Mueller matrices representing different depolarizers based on retarders. Afterwards, we calculate the IPP values of these matrices according to the calculus given Section 2. As in the previous case, depolarization response of the simulated systems is independent of the mean orientation of the retarders, as system rotations do not represent changes in its physical properties. Therefore, the mean orientation of the unit retarders is arbitrarily set to $\overline{\theta}$= 60º in conducted simulations.

In Fig. 2 the values of P_1 and P_2 vary from 0 to 1 depending on the combination of (σ_θ, ϕ), whereas P_3 is always 1. Therefore, as it happened in the case of systems consisting of dichroic elements, systems based on linear retarders are not able to decrease the value for P_3. In terms of Purity Space, different depolarizers consisting of linear retarders are distributed as well within the plane P_3=1. As already discussed in the diattenuation section, due to this restriction of P_3=1 in the retardance case we cannot achieve an ideal depolarizer (*diag(1,0,0,0)*) by simply varying the parameter values in the retardance model, as it is not contained in such a plane.

Unlike the previous case, where P_1 and P_2 showed a very similar behavior (just modified by a vertical shift), in the case of linear retarder based systems, the P_1 shows one minimum valley instead of the two shown by the P_2 channel (i.e. the P_1 distribution between ϕ [0–360º] range occurs as well for the P_2 channel, but in the ϕ [0–180º] range, and it is doubled in the ϕ [0–360º] range). Obviously, according to inequality shown in Eq. (2), the vertical shift in P_2 with respect P_1 is also present. In detail, for retardances ϕ lower than 40º and higher than 320º the simulated samples become non depolarizing (yellow color) independently of the σ_θ value, having P_1=P_2=P_3=*1*. This is because for values of retardance ϕ close to 0º and 360º, Eq. (9) becomes the identity, and therefore, the resulting systems loss their depolarizing capability. Interestingly, as we go far from such values, retardance behavior becomes significant and the resulting systems become depolarizers (going gradually from yellow to blue in Fig. 2(a) and (b)). In particular, depolarizing behavior of systems is achieved for values of ϕ in the range (40º–320º). Within this scenario, the orientation disorder of the retarders units (given by the parameter σ_θ) becomes significant, and depolarization is observed for σ_θ values larger than 20º: P_1 taking values from 0.9 to 0 and P_2 from 1 to 0.

In analogy to diattenuators, it seems that there is a limit value of σ_θ, above which depolarization does not increase. For the case of retarders, such limit value is around 20º (see more details in Section 5 of the supplementary text).

Note that, for values of ϕ close to 180º, P_1 becomes 0 and P_2 is equal to 1. In this case, the Eq. (9) becomes *diag(1,1,−1,−1)*, and therefore, only P_1 is able to differentiate between this case and the above-discussed identity matrix scenario (ϕ=0º or 360º). Accordingly, this difference between P_1 and P_2 can be useful to distinguish between different depolarizers consisting of linear retarders with different retardance ϕ values. For example, a retardance value of ϕ=90º leads to P_1 and P_2 values close to zero, a value of ϕ =180º to P_1=0 and P_2=1 and a value of ϕ=0º or 360º to P_1=1 and P_2=1.

Finally, as a complementary material, in the supplementary text (Fig. S3) we provide the results for further simulated scenarios for the linear retarders case, for instance by adding a variance σ_ϕ (based on a Gaussian probability) to the mean retardance $\overline{\phi}$. Note that even though different simulations lead to different values for P_1 and P_2 channels, in all the cases, the value of P_3 remains always constant to P_3=*1*.

Summarizing, the simulations shown in this subsection further reinforces the idea that depolarizing systems originated by diattenuators or linear retarders microscopic units, are always placed at the top plane (P_3=1 plane) of the tetrahedron of the Purity space. We also observe that P_1 and P_2 parameters strongly depend on the model parameters: attenuations (p_x, p_y), retardance (ϕ) and the variance of the orientation (σ_θ), as well as the diattenuation *D*. These two metrics can be useful to reveal underlying properties of the systems, as if their main constituents are based on diattenuators, linear retarders, or a mix of them. Therefore, they can be used to discriminate between depolarizers based on different linear retarders configurations, or even to differentiate between depolarizers based on dichroic or on linear retarder constituent elements. Under this scenario, a question arises. Which kind of structures are able to decrease the P_3 parameter? This situation is explored in the following section.

4. Depolarizing systems with P_3<1

In practical situations, it is common to find depolarizing systems (both organic and inorganic) with values of P_3 smaller than one, even achieving very low values (close to zero). For instance, in plant and animal tissue we can find P_3 values ranging from 0 to 1 in different structures [24,37]. Note that some of these samples indeed consist of anisotropic elementary components (for instance, animal tissues are mainly based on collagen fibers [38], which can be described by retarders, or vegetal samples are rich in dichroic units [39,40], which can be described by diattenuators).

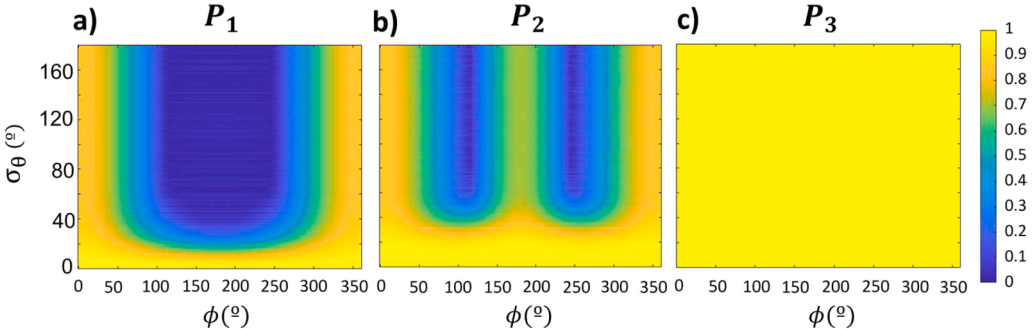

Fig. 2. IPP values for simulated samples composed by linear retarders; (a) P_1, (b) P_2 and, (c) P_3, where x axis represents the mean values of ϕ simulated and, the y axis the variance range values from the from the mean orientation $\overline{\theta}$= 60º.

Recalling the results of previous Section 3, we realize that anisotropic constituent elements in samples cannot explain why all those real samples led to values of $P_3<1$, and therefore, it may exist another depolarizing mechanism to be considered.

Under this scenario, this section focuses on finding a physical mechanism able to describe the depolarizing behavior of real samples with $P_3<1$. We want to note that there are different mechanisms leading to $P_3<1$, but we only focus on those that seem more adequate to explain the depolarizing behavior of most real samples. Some uncommon exotic mechanisms leading to $P_3<1$ (some of them even not representing physical systems) are provided in Section 2.1 of the supplementary document.

In this section we introduce a new group of simulations that lead to $P_3<1$. As in previous Section 3, they consist of an incoherent addition of a number of M representing basic systems (linear retarders and diattenuators), but now, we add an extra term in the summation, this being the Mueller matrix of a perfect depolarizer with a certain weight (β).

The addition of this term in the simulations is inspired on the characteristic decomposition. As can be seen in Eq. (3), this decomposition describes a general matrix M as the addition of four terms, where each one of them is weighted by a linear combination of the IPP. The first term carries the fully polarized contribution of the system. The second and third terms, represent the depolarizing contribution of 2D and 3D systems [17]. Finally, the last term depends on a perfect depolarizing medium (*diag(1,0,0,0)*), which completely depolarizes any incident polarization state of light independently of its initial polarization state. Interestingly, the IPP corresponding to a perfect depolarizer are $P_1=P_2=P_3=0$, and thus, such systems have the capability of decreasing the P_3 channel [41].

For these reasons, we realize that the addition of a perfect depolarizer contribution to the simulations described in previous Section 3 may lead to a decrease of the P_3 value. Therefore, in the new set of simulations, we add an additional term representing a perfect depolarizing Mueller matrix with a certain weight that can be controlled. In particular, this new system can be written as the incoherent addition of a first term describing the contribution to depolarization originated by anisotropic (linear retarders, diattenuators) constituent elements (and obtained as described in Eq. (4)), with a second term, M_{iso}, representing the perfect depolarizing or isotropic contribution. The resulting M can be written as follows:

$$M = m_{00}\widehat{M} = \sum_{i}^{n'} \alpha_i (m_{00}\widehat{M}_i) + \sum_{j}^{m} \beta_j (m_{00}\widehat{M}_{iso}); \quad \alpha_i, \beta_j \geq 0; \sum_{i=1}^{n'} \alpha_i + \sum_{j=1}^{m} \beta_j = 1, \tag{10}$$

where, $n'+m=n$. Note that as in Section 3, n gives the total number of terms in the summation (we set $n=1500$ once again). Since the M_{iso} is the Mueller matrix of a perfect depolarizer (*diag(1,0,0,0)*) the second term can be written as:

$$\sum_{j}^{m} \beta_j (m_{00}\widehat{M}_{iso}) = \beta m_{00}\widehat{M}_{iso}, \tag{11}$$

where, $\beta = \sum_j^m \beta_j$. Therefore, the Eq. (10) can be expressed as:

$$M = m_{00}\widehat{M} = \sum_{i}^{n'} \alpha_i (m_{00}\widehat{M}_i) + \beta m_{00}\widehat{M}_{iso}. \tag{12}$$

The first term, $\sum_i^{n'} \alpha_i (m_{00}\widehat{M}_i)$, represents the effects of depolarizing systems already described in Section 3, that is, depolarizing systems originated by component elements showing retardance or dichroism, and leading to $P_3=1$. In turn, the new added term, $\beta m_{00}\widehat{M}_{iso}$, corresponds to depolarizing systems that fully depolarize light, independently of the input state of polarization of the illumination, and leading to $P_3=0$. In addition, as discussed before, the depolarization introduced by the $\beta m_{00}\widehat{M}_{iso}$ term cannot relate to systems based on anisotropic constituent elements (retarders, diattenuators, mix of them etc.) and thus, it must be connected with isotropic processes introducing polarimetric randomness, as it is the case of isotropic scattering. For this reason, from now on, let us call the first term of Eq. (12) as the anisotropic depolarization term, and the second term as the isotropic depolarization term.

The relation between P_3 and the new added term in the simulation is studied by a set of simulations. By following such Eq. (12), as in previous Section 3, we have access to different control parameters (orientations, retardances, absorption coefficients, deviations, etc.) involved in the anisotropic term, but now, we also control the isotropic component relevance through the weight of the parameter β. We conducted a full space of simulations by repeating the cases analyzed in previous Section 3, but now, by adding the effect of the isotropic term. For the sake of simplicity, in the following we only show and discuss simulations corresponding to a particular case, the incoherent addition of linear diattenuators (Section 3.1) but generalized by the isotropic term. Further simulations results (retarders, combination of linear diattenuators and retarders, etc.) generalized with the isotropic term, can be found in the supplementary text (see Fig. S6), but main conclusions are analogous for all these cases.

Simulated results corresponding to the case of linear diattenuator systems (anisotropic term) incoherently added with the isotropic term are shown in Fig. 3. Results are given in terms of the P_3 metric, P_1 and P_2 have the same dependence with the anisotropic term parameters as in the previous section. As the value of β increases (i.e. P_3 decreases), the value of P_1 and P_2 also decrease (see Eq. (2)) but maintaining the dependence with the anisotropic parameters. To implement the corresponding simulations, the control parameters associated to the anisotropic term were set as: absorption coefficient in the x direction, p_x, set to *1*, mean orientation of linear diattenuators, $\overline{\theta}$, set to 60º, absorption coefficient in the y direction, p_y, taking values from 0 to 1 (values of x axis) and, orientation deviation from mean value, σ_θ, taking values from 0º to 180º (values of y axis). In addition, from Fig. 3(a) to (e) the weight of the isotropic term, β (see Eq.(12)), increases in steps of 0.2 from $\beta=0$ to $\beta=1$.

In Fig. 3 we see that, as expected, the P_3 metric does not depend on the control parameters of the anisotropic term, i.e., all the images in Fig. 3 show a homogeneous color (i.e., present the same value for P_3), because P_3 values are independent of x and y axes values. This situation occurs independently of the anisotropic term control parameters chosen for x and y axes and the elements conforming this term (see Sections 2.2 and 6 of the supplementary material). Unlike this, the values of the isotropic weight, β, control the values of the P_3 Purity parameter (see Fig. 3(a)–(c)). In particular, as larger the β value as shorter the P_3 (note the colorbar in Fig. 3). For the sake of clarity, we also provide Fig. 3(d) where we directly represent the relation between β and P_3, where we note an inverse linear relation between these two parameters. We want to note that the values for the p_x and σ_θ selected for the simulations are arbitrary and we could set other values within the range of the parameters: p_x [0,1] and σ_θ [0,180]. Nevertheless, the main conclusions would remain the same. According to Eq. (12), results in Fig. 3(d) have been obtained from a Mueller matrix composed by an anisotropic part (incoherent addition of diattenuators) and the isotropic part (*diag (1,0,0,0)*). To cover all the possible range of P_3 values, we conduct simulations with β from 0 to 1. This situation confirms that the amount of isotropic scattering in samples is described by the P_3 metric and is directly related to the weight of the isotropic term in Eq. (12). Moreover, since $\widehat{M}_3 = \widehat{M}_{iso}$, by comparing Eq. (12) with the characteristic decomposition (Eq. (3)) we can find the following relation:

$$\beta m_{00}\widehat{M}_{iso} = (1-P_3)(m_{00}\widehat{M}_3) \tag{13}$$

and thus, β = 1- P_3 (note that this result is in agreement with previous Fig. 3(d)). In this way, we find the relation between the weight of the

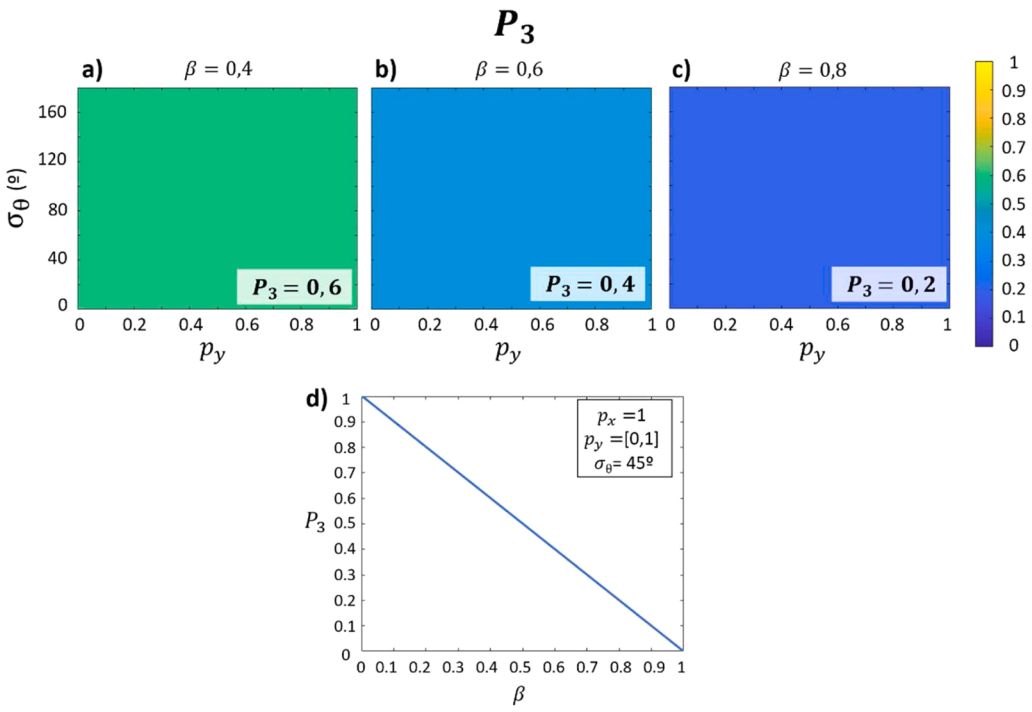

Fig. 3. P_3 values for the simulated samples composed by the incoherent addition of linear diattenuators and a pure depolarizing component with different weights: β=0.4 (a), β=0.6 (b) and β=0.8 (c). The x axis represents the mean value of p_y (where p_x=1) and the y axis the variance range values of the orientation (σ_θ) from 0° to 180°. (d) Relation between β and P_3 obtained from a Mueller matrix with isotropic and anisotropic component, the weight of each component is given by the β value and the parameters that control the anisotropic term are set as p_x=1, σ_θ=45° and p_y varies in the range [0,1].

isotropic contribution, β, with P_3. Moreover, considering the relation between α_i and β weights in Eq. (10), together with β= 1- P_3, we obtain:

$$1 = \sum_{i=1}^{n'} \alpha_i + \beta = \sum_{i=1}^{n'} \alpha_i + (1 - P_3) \rightarrow \sum_{i=1}^{n'} \alpha_i = P_3. \tag{14}$$

By taking into account these results, we can reformulate the weights of the two terms in Eq. (12) just as a function of P_3. To this aim, we define a normalized Mueller matrix $\widehat{M}_A$ in the following way:

$$\sum_{i}^{n'} \alpha_i M_i = P_3 \widehat{M}_A \rightarrow \widehat{M}_A = \frac{1}{P_3} \sum_{i}^{n'} \alpha_i M_i. \tag{15}$$

This relation allows us to re-write Eq. (12) as:

$$M = P_3 m_{00} \widehat{M}_A + (1 - P_3)(m_{00} \widehat{M}_3), \tag{16}$$

where, $\widehat{M}_A$ is defined by Eq. (15) and $\widehat{M}_3 = \widehat{M}_{iso}$. Note that considering the equivalence of Eqs. (16) and (12), the first term, $m_{00}\widehat{M}_A$, is the anisotropic term; and the second term, $m_{00}\widehat{M}_3$, is the isotropic term, and their significance in the incoherent addition is controlled by the Purity term P_3.

Under this scenario, we can say that P_3 controls the depolarizing origin of samples. When P_3=1 the isotropic term is zero (no isotropic depolarization is present), and thus, all the depolarization behavior of samples is given by the anisotropic term, hence, depolarization is originated by the intrinsic polarimetric anisotropies of the sample. In contrast, for P_3=0, the anisotropic term is cancelled and polarimetric anisotropies of constituent elements do not contribute to the depolarizing behavior. In such a case, all depolarization is due to the isotropic term, and corresponding samples behave as perfect depolarizers, originated by processes such as isotropic scattering. In the regime $0<P_3<1$ both depolarizing origins (isotropic and anisotropic) coexist, and the predominant effect is set by the value of P_3.

In addition, recalling the discussion provided in Section 3, the Purity terms P_1 and P_2 complement the information of P_3, as they are able to provide further information about intrinsic characteristics of depolarizing samples based on anisotropic component elements (anisotropic term). In particular, they can estimate if anisotropic depolarization is related to constituent elements showing retardance and/or dichroism and anisotropic scattering produced by these elements. Therefore, the larger the value of P_3, the more relevant become P_1 and P_2 metrics. In this vein, is interesting to note the particular case where P_3=P_2=P_1. In this case, if we study the terms in the characteristic decomposition Eq. (3) the two terms corresponding to the M representing the anisotropic information of the sample disappear. Therefore, this particular case represents a sample where the depolarization is due only to isotropic processes and the parts of the sample representing M_A only contribute to the non-depolarizing term.

Summarizing, in this section we have demonstrated that the depolarizing response of samples can be categorized in two subgroups: (1) those originated by isotropic processes; and (2) those originated by anisotropic processes. These two origins can be produced simultaneously in samples, but their significance can be studied in terms of the Indices of Polarimetric Purity (P_1, P_2 and P_3 metrics). On the one hand, the P_3 metric gives a measure of the presence of depolarization behavior originated by isotropic processes. On the other hand, by considering results provided in Section 3, the metrics P_1 and P_2 complete this information by describing characteristics of anisotropic origin of depolarization (as dichroism, retardance, or a mixture of them). Moreover, the difference between the IPP (P_2-P_1 and P_3-P_2) gives information about the amount of anisotropic depolarization: more difference between the IPP implies more anisotropic depolarization, representing only isotropic depolarization processes when such difference is zero (i.e., P_1=P_2=P_3 case). More insight in this topic can be obtained by studying how a particular depolarizer depolarizes the fully polarized states of polarization at the surface of the Poincaré Sphere and study this situation in terms of IPP [17,42]. A brief discussion in this regard is also provided in Supplementary material.

Note that this is a fundamental result providing which phenomenon originates and/or dominates sample depolarization. In this vein, the association of physical mechanisms leading to depolarization with particular values of IPP provides further description, categorization, and recognition of depolarizing systems, these being very common in both biologic and synthetic materials [6,13,23–25,43,44]. More importantly, this intrinsic microscopic information of samples can be obtained from very feasible macroscopic measurements (measure of Mueller matrix

image).

5. Experimental results

In this section we present simple experiments based on basic polarimetric elements to validate the simulations and conclusions described in Sections 3 and 4. To do so, we obtain the experimental Mueller matrix resulting from the incoherent addition of experimental Mueller matrices of representative polarimetric elements. From these obtained M, we can calculate the corresponding IPP values and compare them with the results corresponding to the stated simulations. On the one hand, in Section 5.1 we present two experimental scenarios corresponding to the $P_3=1$ case (one of them based on dichroic systems and the other based on retarders), and thus, representing anisotropic depolarizing systems to be compared with simulations in Section 3. On the other hand, in Section 5.2, the experimental M of different scattering media are measured to mimic the $P_3<1$ scenario, i.e., the isotropic depolarizing performance of systems, and thus, to be compared with simulations in Section 4. To measure the experimental M of the samples of interest, we use an image Mueller polarimeter [45] described in Section 3 of the supplementary document. In this way, we can compare the experimental and simulated values of the IPP in each case analyzed.

5.1. Experimental results for the $P_3=1$ case

In this section we mimic simulated scenarios described in Section 3, representing anisotropic depolarizing systems.

In the first experiment, we measured the Mueller matrix image of a radial polarizer (from Codixx), which consists of an element including 12 different spatial sectors presenting each a linear polarizer with a different orientation (see Fig. 4(a)). Under this scenario, each pixel of the M image can be understood as a linear polarizer whose orientation is that of the corresponding spatial sector. Afterwards, we set a Region Of Interest (ROI) centered at the intersection of all the sectors (see blue square in Fig. 4(a)), which include 344×471 pixels, including all the 12 linear polarizer orientations. Finally, the Mueller matrices of all the pixels within this ROI are added, this mimicking the incoherent addition of linear polarizers with different orientations simulated in 3.1 (i.e., the M of each pixel is one of the M_i in Eq. (4)). This element can be considered as a diattenuator with large p_x value (we can consider it almost as 1) and low p_y value (we can consider it almost as zero). The orientation angle varies between 0 and 2π through the different sectors. The region selected for the calculations is centered and includes all the polarizer sectors, having therefore a 2π variation of the orientation angle.

The second experiment consist of measuring the Mueller matrix of a liquid crystal q-plate (model WPV10-633 from Thorlabs). This element is a patterned liquid crystal plate that can be understood as a linear retarder with a fixed retardance which depends on the illuminating wavelength (ideally of π radians for the wavelength of 633 nm) and whose neutral axes orientation changes with the spatial position, achieving orientations between 0 and 2π [45] (see Fig. 4(b)). Once again, the M image is calculated, and all the Mueller matrices for the pixels within a ROI with 344×471 pixels (see red rectangle in Fig. 4(b)) are added. Note that this process mimics the scenario discussed in Section 3.2, where different linear retarders with different orientations are incoherently added. Once again, the Mueller matrices within a set ROI (see Fig. 4) are added to construct the incoherent addition of different linear retarders. Therefore, with the q-plate case, by adding the Mueller matrices of the different ROI pixels, we are obtaining the M_i terms in the incoherent addition of a linear retarder with different orientations.

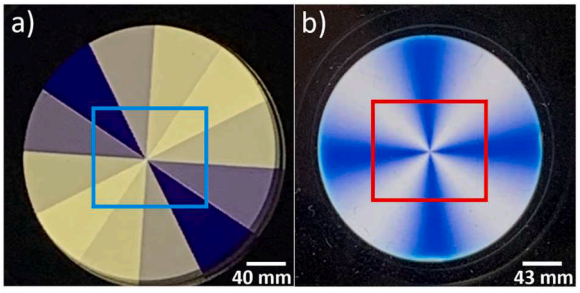

Fig. 4. (a) Radial polarizer illuminated with linear polarization (45°), where each of the sectors indicates a different linear polarizer orientation (between 0 and 2π); each color in the polarizer sector represents a change in orientation of 30° with respect the previous sector. (b) Q-plate image; linear retarder (phase π for 633 nm of illumination) with different orientations, between 0 and 2π represented by the color change in the Figure. In both cases, to see intensity variations associated with different orientations the elements are sandwiched between two crossed polarizers.

In Table 1 we present the IPP results for the above-stated radial polarizer and q-plate experiments. The results provided correspond to the Mueller matrices obtained with illumination at 660 nm wavelength. The samples were measured at different wavelengths giving results in agreement (with the simulated samples) with the presented here. Note that by computing the IPP of the M obtained by performing the incoherent addition of the pixels in both the radial polarizer and the q-plate we obtain values in agreement with the simulations in Section 3, where anisotropic depolarizing ($P_3=1$) systems were analyzed. In both cases, we obtain depolarizing systems, since P_1 and P_2 have values lower than one. However, as expected, the value of P_3 is one for both samples. These results are consistent with the discussion provided in Section 3, where we demonstrated that depolarization originated by unitary elements with polarizing features (dichroism or birefringence; related to physical anisotropies), are reflected on P_1 and P_2 channels, but P_3 was equal to 1 in all the cases (anisotropic depolarization). Moreover, we can consider the radial polarizer as a diattenuator with high p_x and low p_y values, leading to low values for P_1 and high values for P_2. For the q-plate, since the retardance is almost 180° for the illumination wavelength, we also expect a low value for the P_1 parameter and a high value for P_2. In addition, we want to note that we chose different regions (in size and position) for the calculations, where different regions can imply different orientation variations. These results were in accordance with the presented here, also obtaining values of P_3 equal to 1. In turn, as discussed in Section 4, scattering processes lead to isotropic depolarization, and a signature in P_3 channel with values lower than 1. This situation is experimentally validated in the following subsection.

5.2. Experimental results for the $P_3<1$ case

In this section we provide experimental evidence of the $P_3<1$ case, i.e., samples showing isotropic depolarization. These experimental scenarios are based on isotropic scattering processes and validate the simulations performed in Section 4. To this aim, we chose samples composed by elements producing isotropic scattering processes, and thus, that present some contribution of the $M=diag(1,0,0,0)$ type.

The first sample is a diffuse reflector (Diffuser DG10-220-P01, from Thorlabs) consisting in a N-BK7 substrate with a with a rough surface coated with a silver thin film. This roughness diffuses light in all directions and acts as a source with a high degree of isotropic depolarization, as we will show next. For the second sample we chose standard white paper, which is composed by sheets of a mat of random

Table 1
IPP results of the experimentally measured samples representing the incoherent addition of linear polarizers with different orientations and the incoherent addition of linear retarders with different orientations.

	P_1	P_2	P_3
Radial polarizer	0.163	0.876	1
Q plate	0.288	0.727	1

interwoven cellulose fibers with different orientations. This randomness in the paper composition makes it another possible source of isotropic scattering.

In Table 2 we present the resulting IPP from the experimental Mueller matrix images corresponding to the above-mentioned samples. The results correspond to the M obtained with an illumination beam perpendicular to the surface of the samples, at 1500 nm for the silver diffuse reflector surface and 660 nm for the white paper, and they were measured by the Mueller matrix polarimeter described in the supplementary information. In this case, to compute the IPP values of these samples we chose a ROI centered in the image and calculate the mean value and standard deviation corresponding to each IPP. For the diffuser the ROI was 70×70 pixels and in the case of the white paper it was a 150 x 150-pixel ROI.

As expected, the value of P_3 is different from one in both cases, showing the isotropic nature of the depolarization produced by these samples. Therefore, the composition of the samples makes isotropic scattering the predominant process in their light interaction. In the case of the silver diffuse reflector the value achieved for P_3 is 0.200 and, 0.294 for the white paper. Recalling the inequality related to IPP (see Eq. (2)), values for P_1 and P_2 are restricted to be equal or lower than 0.200 and, 0.294, for the two samples respectively. However, due to the fact that P_3 is not exactly equal to zero, still there is some non-zero values for P_1 and P_2. This situation shows that even though isotropic depolarization is the predominant depolarizing mechanism in these samples, still there is some anisotropic depolarization present. The origin of these anisotropic depolarization must be related with the polarizing properties of the constituent elements. In the case of the white paper, this anisotropic scattering is due to the retardance properties present in the cellulose fibers [39,46]. For the silver diffuse reflector, it can be due to the non ideality of the fabrication process and some intrinsic polarimetric characteristic of the component elements. As for instance, the protection coating (silver) can present dichroic behavior. These intrinsic characteristics of the samples can explain the presence of anisotropic scattering.

Moreover, if we inspect the differences between the IPP values we find that these values are different to zero, that is it (P_1 -P_2) and (P_2 –P_3) achieve values larger than zero for both samples. Taking into account the expression of the characteristic decomposition (Eq. (3)) we can see that the weight of all the terms is different from zero. These weights represent the amount of anisotropic scattering present in the sample (being zero for the case of P_3=P_2=P_1). These results are in concordance with conclusions of Section 4.

In conclusion, with these experimental results we show the concordance of our study of the IPP by means of the simulations of the previous sections. With the experimental results obtained by the measurement of the Mueller matrix of different polarimetric elements we prove the validity of our interpretation of the IPP parameters to characterize the polarization and depolarization response of the sample.

6. Conclusions

In this manuscript we provided the usefulness of the Indices of Polarimetric Purity (IPP) to study depolarizing samples. Previous studies have already shown that the IPP are ideal metrics to be used for the enhanced visualization of structures, as in the case of biological samples. In this manuscript, we focused on the physical interpretation of the IPP, which, in turn, gives physical information about the samples themselves, and in particular, about the intrinsic mechanisms giving rise to depolarization. In this sense, we propose for the first time the concept of isotropic and anisotropic depolarization, as distinct depolarizing origins that can take place simultaneously or separately in samples, and their connection with IPP values. This thorough information of the physical origin of depolarizers is directly obtained from IPP values associated to samples and can be applied in multiple scenarios when dealing with depolarizing samples.

Table 2
Mean values and standard deviation of the samples comprised by an isotropic and anisotropic term.

	$\overline{P}_1 \pm \sigma_{P1}$	$\overline{P}_2 \pm \sigma_{P2}$	$\overline{P}_3 \pm \sigma_{P3}$
Silver diffuse reflector	0.05 ±0.02	0.11 ±0.03	0.20 ±0.04
White paper	0.05 ±0.02	0.14 ±0.04	0.29 ±0.07

The study is based on a series of simulations in Sections 3 and 4 that help to connect the magnitudes of IPP with different scattering sources in light-matter interaction processes. The simulations are based on the incoherent addition of Mueller matrices representing elemental polarimetric samples and give rise to different simulated depolarizers. The physical interpretation of results was also conducted in terms of the characteristic decomposition, which decompose a general Mueller matrix as the addition of four different Mueller matrices (with clear physical interpretation) whose weights are given by combinations of IPP.

Results show that the index P_3 is related with isotropic depolarization, where input light is fully depolarized independently of its polarization. These systems represent samples associated with scattering processes, which may be originated by a wide range of physical processes based on diffuse reflections. In fact, isotropic depolarization is a multiple scattering process where the polarimetric signature is lost (independently of the input polarization, the exiting beam is fully depolarized). This process only connects with the P_3 value.

In turn, we also show that P_1 and P_2 metrics give measure of the anisotropic depolarization processes. Simulations provide that this depolarization is originated by light-matter interactions with anisotropic basic elements (dichroic and/or birefringent) with different orientations or physical magnitudes (transmittances, retardance, etc.). Anisotropic depolarizing media differently affects an input light beam as a function of their state of polarization. Simulations have been experimentally validated by conducting different simple experiments where different polarimetric samples, mimicking the simulated scenarios, where measured and analyzed in terms of IPP. Furthermore, by inspecting the characteristic decomposition (Eq. (3)) and the results of our work we can relate the P_1 and P_2 changes with the polarimetric component units of a sample which are encoded in the M_{J0}, M_1 and M_2 matrices of the stated characteristic decomposition. Note that these three matrices have physical interpretation as stated in the description of above-presented Eq. (3).

In conclusion, by studying the IPP magnitudes associated to a sample, we reveal the physical origins that give rise to depolarization: scattering processes, anisotropic elements or a mix of them. Note that provided results are of crucial importance because they allow us to link depolarization measures at macroscopic scale, with microscopic properties of samples, and with a non-invasive and non-destructive technique (polarimetry).

The present manuscript can be useful for a wide range of applications, where depolarizing samples are involved. In this sense, we put special focus on applications in biophotonics, as organic (vegetal and animal) tissues strongly depolarize incident light. In this regard, different authors have analyzed biological tissues in terms of the IPP. For instance, in Ref. [13] we can see how by means of the IPP channels unwrap new information which was hidden by using other polarimetric channels in different biological samples such as the nutritious channels in an *ex-vivo* rabbit leg and capillaries of the papillary muscles of an *ex-vivo* lamb heart. Also, the different IPP response of samples is highly useful for biological tissue discrimination [25,26], which can be different structures (Ref. [26]) or discrimination between healthy or pathological tissue (Ref. [25]). In all these cases, the information given by IPP relate to methods and discussions presented in the current manuscript.

Therefore, the use of IPP as a tool to study tissues could give relevant information of the interaction of incident light with inherent polarimetric elements in tissues (for instance, different types of collagen,

identified as birefringent elements, or different structures in vegetal samples, identified as dichroic [38]). Under this scenario, for each studied sample, we can evaluate the relevance of diffuse reflections and/or polarizing elements in final depolarizing measures, or more importantly, the spatial depolarizing heterogeneity in such samples, this being applicable to the study of pathological tissues (which modifies internal polarizing properties, organization, etc.).

CRediT authorship contribution statement

Mónica Canabal-Carbia: Writing – original draft, Formal analysis, Software, Conceptualization, Data curation. **Irene Estévez:** Writing – review & editing, Conceptualization. **Esther Nabadda:** Validation, Investigation. **Enrique Garcia-Caurel:** Writing – review & editing, Conceptualization. **J.J. Gil:** Writing – review & editing, Conceptualization. **Razvigor Ossikovski:** Writing – review & editing. **Andrés Márquez:** Writing – review & editing. **Ignacio Moreno:** Writing – review & editing, Validation, Investigation. **Juan Campos:** Project administration, Funding acquisition, Writing – review & editing, Conceptualization, Supervision. **Angel Lizana:** Writing – review & editing, Conceptualization, Project administration, Funding acquisition, Supervision.

Declaration of Competing Interest

The authors declare the following financial interests/personal relationships which may be considered as potential competing interests:

Monica Canabal-Carbia reports financial support was provided by Spain Ministry of Science and Innovation (PID2021-560 126509OB-C21 and PDC2022-133332-C21). Juan Campos reports financial support was provided by Spain Ministry of Science and Innovation (PID2021-560 126509OB-C21 and PDC2022-133332-C21). Angel Lizana reports financial support was provided by Spain Ministry of Science and Innovation (PID2021-560 126509OB-C21 and PDC2022-133332-C21). Irene Estevez reports financial support was provided by Government of Catalonia (Beatriu de Pinos, 2021-BP-00206). Ignacio Moreno reports financial support was provided by Spain Ministry of Science and Innovation (PID2021-126509OB-C22). Andres Marquez reports financial support was provided by Government of Valencia. Andres Marquez reports financial support was provided by Spain Ministry of Science and Innovation (PID2021-123124OB-I00). Esther Nabadda reports financial support was provided by Government of Valencia. Mónica Canabal-Carbia, Angel Lizana and Juan Campos reports financial support was provided by the Generalitat de Catalunya (2021SGR00138).

Data availability

Data will be made available on request.

Acknowledgments

The authors acknowledge the financial support of Ministerio de Ciencia e Innovación and Fondos FEDER (PID2021-126509OB-C21 and PDC2022-133332-C21) and support of Generalitat de Catalunya (2021SGR00138).

IM acknowledge the financial support of Ministerio de Ciencia e Innovación and Fondos FEDER (PID2021-126509OB-C22) AM acknowledges support from project PROMETEO/2021/006 (Generalitat Valenciana, Spain) and PID2021-123124OB-I00 (Ministerio de Ciencia e Innovación, Spain).

EN acknowledges a grant from Generalitat Valenciana, Santiago Grisolia Program (ref. GRISOLIAP/2020/004).

IE acknowledges financial support from a Beatriu de Pinós Fellowship (2021-BP-00206).

Supplementary materials

Supplementary material associated with this article can be found, in the online version, at doi:10.1016/j.optlaseng.2023.107830.

References

[1] Honda M, Tazaki R, Murakawa K, Terada H, Kudo T, Hattori T, et al. Subaru/IRCS *L* -band spectro-polarimetry of the HD 142527 disk scattered light. Publ Astron Soc Jpn 2022;74:851–6. https://doi.org/10.1093/pasj/psac041.

[2] Asgarimehr M, Hoseini M, Semmling M, Ramatschi M, Camps A, Nahavandchi H, et al. Remote sensing of precipitation using reflected GNSS signals: response analysis of polarimetric observations. IEEE Trans Geosci Remote Sens 2022;60: 1–12. https://doi.org/10.1109/TGRS.2021.3062492.

[3] Richter S, Rebarz M, Herrfurth O, Espinoza S, Schmidt-Grund R, Andreasson J. Broadband femtosecond spectroscopic ellipsometry. Rev Sci Instrum 2021;92: 033104. https://doi.org/10.1063/5.0027219.

[4] Mahmoud NA-E. Analytical study of precision optical glass surface and its effect on some polarimetric parameters. J Surf Eng Mater Adv Technol 2022;12:14–21. https://doi.org/10.4236/jsemat.2022.121002.

[5] Shkirin AV, Ignatenko DN, Chirikov SN, Bunkin NF, Astashev ME, Gudkov SV. Analysis of fat and protein content in milk using laser polarimetric scatterometry. Agriculture 2021;11:1028. https://doi.org/10.3390/agriculture11111028.

[6] Van Eeckhout A, Garcia-Caurel E, Garnatje T, Durfort M, Escalera JC, Vidal J, et al. Depolarizing metrics for plant samples imaging. PLOS One 2019;14:e0213909. https://doi.org/10.1371/journal.pone.0213909.

[7] Rehbinder J, Vizet J, Park J, Ossikovski R, Vanel J-C, Nazac A, et al. Depolarization imaging for fast and non-invasive monitoring of cervical microstructure remodeling *in vivo* during pregnancy. Sci Rep 2022;12:12321. https://doi.org/10.1038/s41598-022-15852-w.

[8] He C, He H, Chang J, Dong Y, Liu S, Zeng N, et al. Characterizing microstructures of cancerous tissues using multispectral transformed Mueller matrix polarization parameters. Biomed Opt Express 2015;6:2934. https://doi.org/10.1364/BOE.6.002934.

[9] Dubreuil M, Tissier F, Rivet S, Le GY. Linear diattenuation imaging of biological tissues with near infrared Mueller scanning microscopy. Biomed Opt Express 2021; 12:41. https://doi.org/10.1364/BOE.408354.

[10] Menzel M, Axer M, Amunts K, De Raedt H, Michielsen K. Diattenuation imaging reveals different brain tissue properties. Sci Rep 1939;9. https://doi.org/10.1038/s41598-019-38506-w. 2019.

[11] Pierangelo A, Benali A, Antonelli M-R, Novikova T, Validire P, Gayet B, et al. *Ex-vivo* characterization of human colon cancer by Mueller polarimetric imaging. Opt Express 2011;19:1582. https://doi.org/10.1364/OE.19.001582.

[12] Du E, He H, Zeng N, Sun M, Guo Y, Wu J, et al. Mueller matrix polarimetry for differentiating characteristic features of cancerous tissues. J Biomed Opt 2014;19: 076013. https://doi.org/10.1117/1.JBO.19.7.076013.

[13] Van Eeckhout A, Lizana A, Garcia-Caurel E, Gil JJ, Sansa A, Rodríguez C, et al. Polarimetric imaging of biological tissues based on the indices of polarimetric purity. J Biophotonics 2018;11:e201700189. https://doi.org/10.1002/jbio.201700189.

[14] Rodríguez C, Van Eeckhout A, Ferrer L, Garcia-Caurel E, González-Arnay E, Campos J, et al. Polarimetric data-based model for tissue recognition. Biomed Opt Express 2021;12:4852. https://doi.org/10.1364/BOE.426387.

[15] Van Eeckhout A, Garcia-Caurel E, Ossikovski R, Lizana A, Rodríguez C, González-Arnay E, et al. Depolarization metric spaces for biological tissues classification. J Biophotonics 2020;13. https://doi.org/10.1002/jbio.202000083.

[16] Ossikovski R, Vizet J. Eigenvalue-based depolarization metric spaces for Mueller matrices. J Opt Soc Am A 2019;36:1173. https://doi.org/10.1364/JOSAA.36.001173.

[17] Gil JJ, Ossikovski R. Polarized light and the Mueller matrix approach. CRC Press; 2022. https://doi.org/10.1201/9780367815578. New York.

[18] Van Eeckhout A, Gil JJ, Garcia-Caurel E, Romero JG, Ossikovski R, José IS, et al. Unraveling the physical information of depolarizers. Opt Express 2021;29:38811. https://doi.org/10.1364/OE.438673.

[19] Gil JJ. Polarimetric characterization of light and media: physical quantities involved in polarimetric phenomena. Eur Phys J Appl Phys 2007;40:1–47.

[20] San José I, Gil JJ. Invariant indices of polarimetric purity: generalized indices of purity for n × n covariance matrices. Opt Commun 2011;284:38–47. https://doi.org/10.1016/j.optcom.2010.08.077.

[21] Van Eeckhout A, Lizana A, Garcia-Caurel E, Gil JJ, Ossikovski R, Campos J. Synthesis and characterization of depolarizing samples based on the indices of polarimetric purity. Opt Lett 2017;42:4155. https://doi.org/10.1364/OL.42.004155.

[22] Wang P, Li D, Wang X, Guo K, Sun Y, Gao J, et al. Analyzing polarization transmission characteristics in foggy environments based on the indices of polarimetric purity. IEEE Access 2020;8:227703–9. https://doi.org/10.1109/ACCESS.2020.3045993.

[23] Li X, Zhang L, Qi P, Zhu Z, Xu J, Liu T, et al. Are indices of polarimetric purity excellent metrics for object identification in scattering media? Remote Sens 2022; 14:4148. https://doi.org/10.3390/rs14174148 (Basel).

[24] Rodríguez C, Van Eeckhout A, Garcia-Caurel E, Lizana A, Campos J. Automatic pseudo-coloring approaches to improve visual perception and contrast in polarimetric images of biological tissues. Sci Rep 2022;12:18479. https://doi.org/10.1038/s41598-022-23330-6.

[25] Ivanov D, Dremin V, Borisova E, Bykov A, Novikova T, Meglinski I, et al. Polarization and depolarization metrics as optical markers in support to histopathology of *ex vivo* colon tissue. Biomed Opt Express 2021;12:4560. https://doi.org/10.1364/BOE.426713.
[26] Rodríguez C, Estévez I, González-Arnay E, Campos J, Lizana A. Optimizing the classification of biological tissues using machine learning models based on polarized data. J Biophotonics 2023;16. https://doi.org/10.1002/jbio.202200308.
[27] Gil JJ, Bernabeu E. Depolarization and polarization indices of an optical system. Opt Acta Int J Opt 1986;33:185–9. https://doi.org/10.1080/713821924.
[28] Goldstein DH. Polarized light. CRC Press; 2017. https://doi.org/10.1201/b10436.
[29] Chipman R.A. Polarimetry. Chapter 22 in handbook of optics II 1995.
[30] Gil JJ. Structure of polarimetric purity of a Mueller matrix and sources of depolarization. Opt Commun 2016;368:165–73. https://doi.org/10.1016/j.optcom.2016.01.092.
[31] Ossikovski R, Gil JJ. Basic properties and classification of Mueller matrices derived from their statistical definition. J Opt Soc Am A 2017;34:1727. https://doi.org/10.1364/JOSAA.34.001727.
[32] Gil JJ, San José I. Information structure and general characterization of Mueller matrices. J Opt Soc Am A 2022;39:314. https://doi.org/10.1364/JOSAA.448255.
[33] Cloude S. Group theory and polarisation algebra. Optik 1986;75:26–36 (Stuttg).
[34] Gil JJ, José IS. Arbitrary decomposition of a Mueller matrix. Opt Lett 2019;44:5715. https://doi.org/10.1364/OL.44.005715.
[35] Gil JJ. Components of purity of a three-dimensional polarization state. J Opt Soc Am A 2016;33:40. https://doi.org/10.1364/JOSAA.33.000040.
[36] Ossikovski R, Arteaga O, Garcia-Caurel E, Hingerl K. Model for the depolarizing retarder in Mueller matrix polarimetry. J Opt Soc Am A 2022;39:873. https://doi.org/10.1364/JOSAA.451106.
[37] Canabal-Carbia M, Van Eeckhout A, Rodríguez C, González-Arnay E, Estévez I, Gil JJ, et al. Depolarizing metrics in the biomedical field: vision enhancement and classification of biological tissues. J Innov Opt Health Sci 2023. https://doi.org/10.1142/S1793545823300045.
[38] Wang LV, Coté GL, Jacques SL. Special section guest editorial. J Biomed Opt 2002;7:278. https://doi.org/10.1117/1.1489434.
[39] Al BB, Y Su, Rodríguez C, Lizana A, Campos J, Durfort M, et al. Characterization of vine, Vitis vinifera, leaves by Mueller polarimetric microscopy. Thin Solid Films 2023;764:139594. https://doi.org/10.1016/j.tsf.2022.139594.
[40] Breton J, Michel-Villaz M, Paillotin G. Orientation of pigments and structural proteins in the photosynthetic membrane of spinach chloroplasts: a linear dichroism study. Biochimica et Biophysica Acta (BBA) - Bioenerg 1973;314:42–56. https://doi.org/10.1016/0005-2728(73)90062-5.
[41] Gil JJ. On optimal filtering of measured Mueller matrices. Appl Opt 2016;55:5449. https://doi.org/10.1364/AO.55.005449.
[42] Van Eeckout A. Polarimetric methods for the image enhancement in biological applications. Universitat Autònoma de Barcelona; 2017.
[43] Shen F, Zhang M, Guo K, Zhou H, Peng Z, Cui Y, et al. The depolarization performances of scattering systems based on the Indices of Polarimetric Purity (IPPs). Opt Express 2019;27:28337. https://doi.org/10.1364/OE.27.028337.
[44] Li D, Guo K, Sun Y, Bi X, Gao J, Guo Z. Depolarization characteristics of different reflective interfaces indicated by Indices of Polarimetric Purity (IPPs). Sensors 2021;21:1221. https://doi.org/10.3390/s21041221.
[45] López-Morales G, Sánchez-López M, Lizana Á, Moreno I, Campos J. Mueller matrix polarimetric imaging analysis of optical components for the generation of cylindrical vector beams. Crystals 2020;10:1155. https://doi.org/10.3390/cryst10121155 (Basel).
[46] Palevitz BA, Hepler PK. Cellulose microfibril orientation and cell shaping in developing guard cells of Allium: the role of microtubules and ion accumulation. Planta 1976;132:71–93. https://doi.org/10.1007/BF00390333.